

We are IntechOpen, the world's leading publisher of Open Access books Built by scientists, for scientists

5,800

Open access books available

142,000

International authors and editors

180M

Downloads

Our authors are among the

154

Countries delivered to

TOP 1%

most cited scientists

12.2%

Contributors from top 500 universities



WEB OF SCIENCE™

Selection of our books indexed in the Book Citation Index
in Web of Science™ Core Collection (BKCI)

Interested in publishing with us?
Contact book.department@intechopen.com

Numbers displayed above are based on latest data collected.
For more information visit www.intechopen.com



Advanced Manufacturing for Bone Tissue Engineering and Regenerative Medicine

Roozbeh (Ross) Salary

Abstract

This book chapter delineates advanced additive manufacturing processes used in clinical practice for high-resolution fabrication of mechanically-robust and dimensionally-accurate bone tissue scaffolds with a focus on pneumatic micro-extrusion, fused deposition modeling, polymer jet printing, and digital light processing. The main components as well as the underlying physics behind each process are explained. Furthermore, this chapter is integrated with a review of literature; the aim is to show how these additive manufacturing processes are potentially utilized in clinical practice for bone tissue engineering. This chapter serves as an introductory platform toward advanced studies and/or research works in the area of bone regenerative medicine. Finally, this chapter will be helpful to engineering and medical students as well as researchers from academia and industry.

Keywords: bone tissue engineering, regenerative medicine, advanced manufacturing

1. Introduction

1.1 Objective and scope

The objective of this chapter is to introduce AM processes, which have been utilized in clinical practice for the fabrication of mechanically-robust and dimensionally-accurate bone tissue scaffolds for the treatment of osseous fractures, defects, and diseases (such as osteoporosis, bone tumor resection, and orthopedic trauma). Particularly, this chapter concentrates on PME, FDM, PJP, as well as DLP with a special focus on the PME-AM process. **Figure 1** illustrates additively-manufactured biocompatible bone tissue scaffolds and constructs having porous internal structures. Please note that the phantom as well as the femur bone were composed of a medical-grade composite material [1, 2], while the cubic microporous scaffold was composed of PCL [3–5].

The aforementioned AM processes enable high-resolution, non-contact, and multi-material deposition of functional bio-inks, polymer materials, as well as composite materials for tissue engineering applications. In spite of their benefits and potential applications, the AM processes are intrinsically complex. The process complexity, to a great extent, stems from not only complex physical phenomena (such as phase change and non-Newtonian material deposition), but also dynamic material-process interactions. In addition, there are a broad range of design factors and process parameters (such as porosity, surface roughness, scaffold topology,

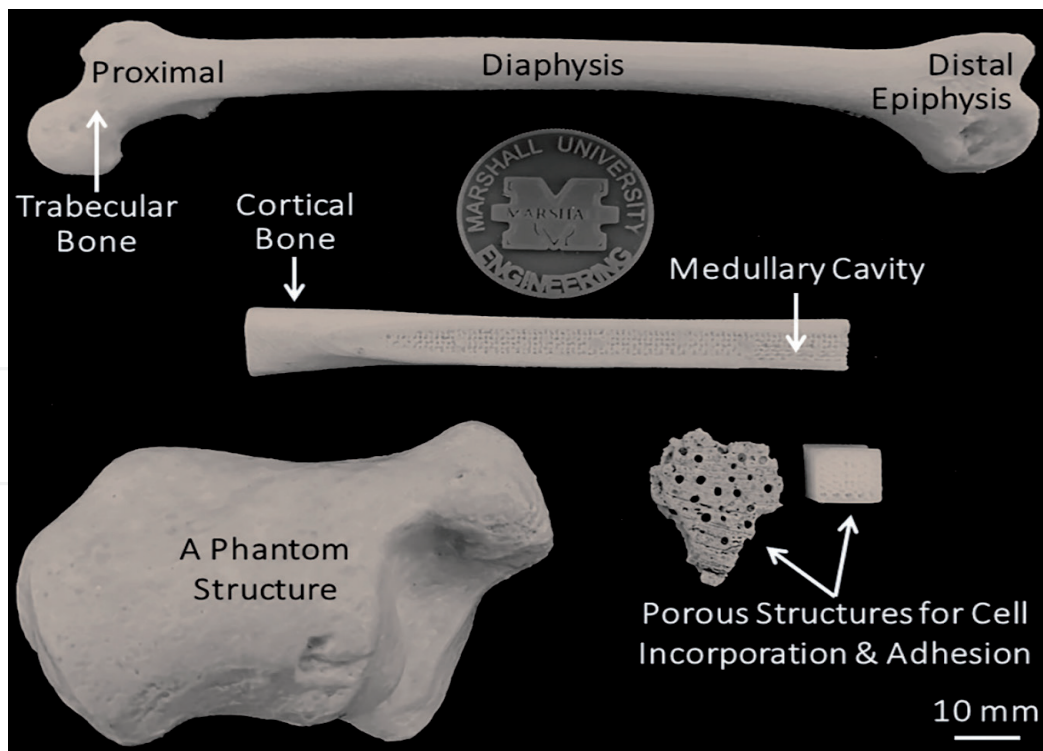


Figure 1. Biocompatible bone scaffolds and constructs with microporous internal structures, which allow for not only cell incorporation and adhesion, but also diffuse proliferation for clinical practice (Source: [1–5]).

nozzle diameter, material viscosity, as well as material deposition pressure, flow rate, and temperature) that contribute to the complexity of the AM processes. Consequently, investigation of the influence of the significant design and process parameters (in addition to their interactions) on the mechanical, biomedical, and morphological properties of the fabricated bone structures would be inevitable [1–10]. In the absence of such knowledge, orthopedic surgeons and clinicians will be unable to efficiently treat osseous fractures in the presence of constraints, such as sex, age, bone density, and immune system rejection. Hence, the aim of this chapter is to introduce the AM processes and highlight their significant process parameters. The PME, FDM, PJP, and DLP processes will be reviewed in Sections 2.1–2.4, respectively. A review of other AM processes (i.e., powder bed fusion as well as binder jetting) used in clinical practice is given in Section 2.5. Finally, the conclusions are presented in Section 3.

2. AM processes for bone tissue engineering

2.1 Pneumatic micro-extrusion (PME)

PME is a material extrusion AM process [11], which has emerged as a robust high-resolution method for the fabrication of a wide range of biological tissues, scaffolds, and structures. Advanced PME systems, for example, Cellink BIO X (Boston, MA, USA), have a layer resolution and positioning precision of 100 and 10 μm , respectively.

As demonstrated in **Figure 2**, the PME process utilizes a high-pressure gas flow (typically air, supplied by a compressor) as a medium of transport and deposition. A polymer material (typically in powder form) is loaded into the deposition head's cartridge (also known as barrel) and subsequently heated above the polymer's melting temperature; this results in formation of a non-Newtonian molten

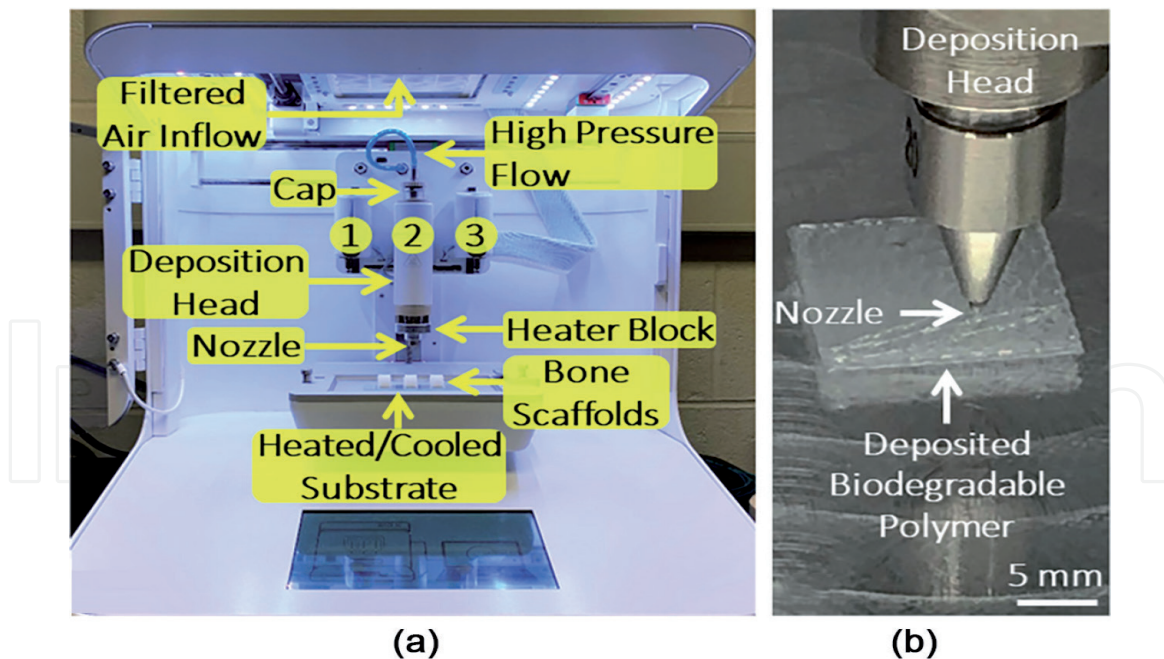


Figure 2.
(a) The material deposition chamber as well as the main components of the PME AM process; and
(b) pneumatic micro-deposition of a polymer material (PCL) on a heated glass substrate using a converging microcapillary nozzle (Source: [3–5]).

polymer flow prior to deposition [3–5]. An internal/external air compressor or a pressure source (not shown), provides a steady pressure flow into the cartridge. Having high thermal conductivity, the cartridge allows for rapid melting of the loaded polymer material. The molten polymer is, subsequently, deposited on a heated/cooled free surface via a converging microcapillary nozzle with the aid of the pressurized gas flow. A fan with a filter at the top of the chamber not only delivers a clean air flow, but also aids in maintaining a fixed level (rate) of polymer solidification (and thus layer adhesion). The surface temperature is kept below the melting temperature of the polymer material. Spoerk et al. [12] observed that an optimal bed temperature would be critical for proper layer adhesion and thus accurate material deposition.

Klemstine et al. [3] investigated the mechanical properties of biocompatible and biodegradable triply periodic minimal surface-based bone scaffolds, composed of PCL and fabricated using the PME-AM process. Having a molecular weight (M_n) as well as a density of approximately 50,000 and 1.145 g/mL (at 25°C), respectively, PCL is a semi-crystalline, hydrophobic polyester-based polymer, derived from caprolactone monomer using ring-opening polymerization. It has a glass transition temperature of -60°C and a melting temperature in the range of $59\text{--}64^\circ\text{C}$. In addition, PCL has a tensile strength and elasticity modulus (indicative of stiffness) of 16 MPa and 0.4 GPa, respectively [13]. The PME fabrication of the bone scaffolds was on the basis of a set of optimal process parameters, detailed in **Table 1**.

In a research work, Yu et al. [4] investigated the effects of influential scaffold design factors and process parameters—as listed in **Table 2**, including layer thickness, layer width, infill density, print speed, flow pressure, deposition head temperature, and infill pattern—on the dimensional accuracy as well as the mechanical properties of PME-fabricated PCL bone scaffolds. The assessment of the scaffold dimensional accuracy was based on not only a digital image processing platform established in the MATLAB environment, but also physical measurements (used to corroborate the veracity of the image-based assessment). The underlying algorithms embedded in the image-processing platform are discussed in detail in [14, 15].

Parameter	Type	Level [unit]
Layer height (thickness)	Design	200 [μm]
Infill pattern	Design	Concentric
Nozzle size	Machine	200 [μm]
Bed temperature	Machine	10 [$^{\circ}\text{C}$]
Print speed	Machine	2.5 [mm/s]
Deposition head temperature	Machine	180 [$^{\circ}\text{C}$]
Deposition flow pressure	Machine	300 [kPa]
Pre-flow delay	Machine	900 [ms]
Post-flow delay	Machine	400 [ms]

Table 1.

The optimal PME process parameters used by Klemstine et al. for the additive fabrication of biocompatible bone scaffolds composed of PCL. Please note that the bone scaffold fabrication process was based on the Cellink BIO X 3D-bioprinting system (Source: [3]).

Parameter	Type	Level [unit]
Variables		
Layer height/thickness	Design	125–200 [μm]
Layer/line width	Design	125–200 [μm]
Print speed	Machine	0.30–0.45 [mm/s]
Infill density	Design	0.20–0.35
Deposition head temperature (DHT)	Machine	100–125 [$^{\circ}\text{C}$]
Flow pressure	Machine	520–560 [kPa]
Infill pattern	Design	• Honeycomb; • Rectilinear; • Concentric; • Cubic; • Gyroid.
Fixed parameters		
Filling/raster angle	Design	90 [$^{\circ}$]
Number of shells	Design	2
Scaffold diameter	Design	10 [mm]
Scaffold height	Design	3 [mm]
Nozzle size	Machine	200 [μm]
Bed temperature	Machine	45 [$^{\circ}\text{C}$]
Fan speed	Machine	100 [%]

Table 2.

The experimental design table established by Yu et al. to systematically study the influence of seven design and process parameters on the functional properties of PCL bone scaffolds fabricated using the PME process. Please note that the bone scaffold fabrication process was based on the Cellink INKREDIBLE⁺ 3D-bioprinting system (Source: [4]).

Please note that the image-processing platform, in addition, allows for *in situ* characterization, monitoring, and ultimately control of the PME process.

Figure 3 illustrates the influence of the deposition head temperature (as an example of the PME process parameters) on the morphology as well as the micro-structure of the fabricated PCL bone scaffolds. It is implied from the figure that the scaffold diameter increases as a result of an increase in the deposition head

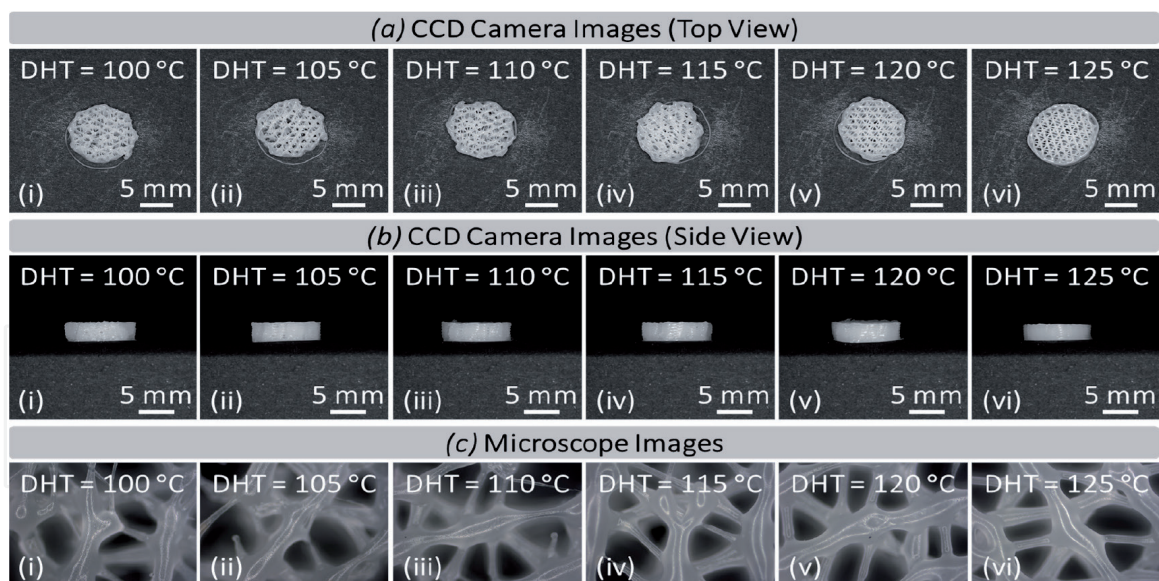


Figure 3. The influence of deposition head temperature (DHT) at six levels of 100, 105, 110, 115, 120, and 125 °C on: (a, b) the morphology, and (c) the microstructure of PME-fabricated PCL bone scaffolds (Source: [4]).

temperature. This phenomenon, largely, stems from the fact that an increase in the deposition head temperature leads to a decrease in the polymer viscosity and consequently, an increase in material deposition rate (resulting in formation of larger bone scaffolds in diameter). Besides, Yu et al. [4] observed that the scaffold stiffness increased when the deposition head temperature increased from 100 to 125 [°C]; this trend can be due to the increased amount of deposited mass per scaffold structure as a result of a decline in the polymer viscosity (when the deposition head temperature increases).

Yeow et al. [4, 8] developed a 3D computational fluid dynamics (CFD) model with the aim to investigate the underlying non-Newtonian fluid dynamics of material transport and deposition in the PME process, formulated as a transient multi-phase flow problem. Demonstrated in **Figure 4(a)**, the geometry of the CFD model consisted of a cartridge, a connector, as well as a microcapillary nozzle (having a diameter of 200 μm). It turned out that approximately five layers of inflation would be sufficient to obtain accurate solution near the wall boundaries. Shown in **Figure 4(b)**, four boundary conditions were defined for the CFD model, including flow pressure inlet, stationary wall, volume fraction, and pressure outlet. Both the energy equation and the laminar viscous model were included in the CFD model (in addition to the continuity and momentum equations) respectively to account for the effects of viscous heating and to capture the effects of viscosity.

It was observed that the transport of molten PCL through the micro-capillary nozzle (under a flow pressure of 550 kPa) would be a viscous flow having a Reynolds number (Re) of $\ll 1$, implied from **Figure 4(c)**. This PME material deposition regime is unlike that of the other additive manufacturing processes, such as AJP, where material deposition is intrinsically turbulent [14, 16, 17].

The following research works exemplify the use of PME in clinical practice. In a research work, Du et al. [18] demonstrated additive fabrication of mesoporous bioactive glass/silk fibroin composite scaffolds with high osteogenic ability using the PME process. The functional properties of the fabricated scaffolds were characterized on the basis of porosity, compressive strength, degradation, biocompatibility, as well as apatite forming ability. The results of an animal study showed that the mesoporous bioactive glass/silk fibroin composite scaffolds (loaded with human bone marrow mesenchymal stem cells) had not only more significant osteogenic

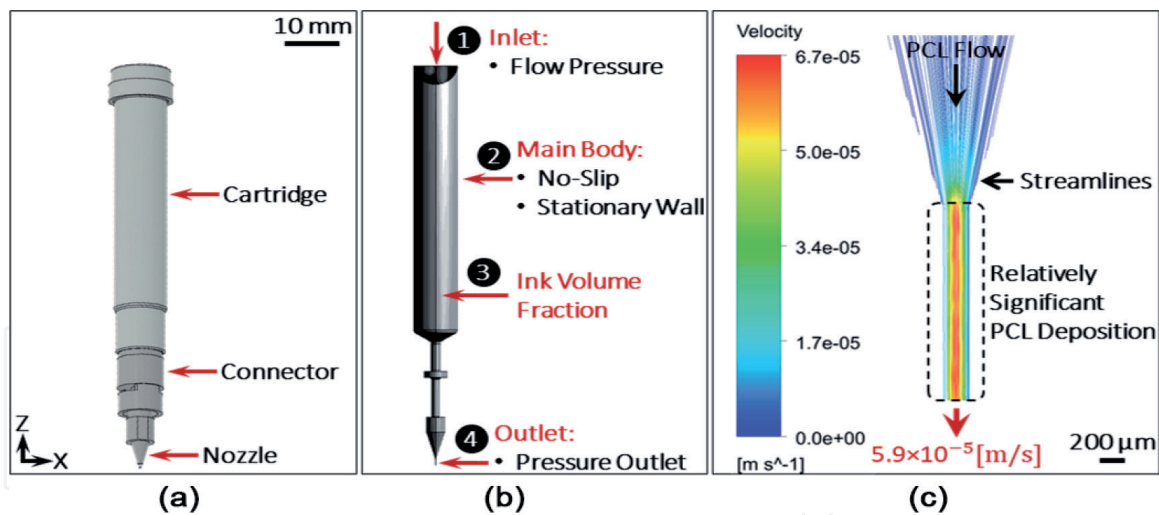


Figure 4. (a) The main components of the PME deposition head assembly; (b) the boundary conditions defined for the 3D-CFD model; and (c) simulation of the velocity field in the PME deposition head under a flow pressure of 550 kPa (Source: [4, 8]).

potential, but also superior compressive strength and biocompatibility than mesoporous bioactive glass/polycaprolactone (PCL) scaffolds.

In addition, Du et al. [19] demonstrated 3D-fabrication of pearl/calcium sulfate composite scaffolds—characterized with high osteogenic ability, uniform interconnected macropores, high porosity, as well as improved mechanical properties—using PME integrated with a hydration process. The fabricated scaffolds not only showed satisfactory apatite-forming ability, but also stimulated the proliferation as well as differentiation of rat bone mesenchymal stem cells. The osteogenic potential of the scaffolds was assessed based on micro-computed tomography (μ -CT) imaging and histological analysis.

Park et al. [20] demonstrate a novel technique, combining 3D printing with spatial-temporal deposition and control of growth factors, with the aim to prevascularize bone tissues. Having osteogenic and vasculogenic potential, human dental pulp stem cells were deposited using the PME process together with bone morphogenetic protein-2 as well as vascular endothelial growth factor. An animal study was conducted where both micro-vessel formation and angiogenesis were observed.

Cui et al. [21] investigated 3D-fabrication of polyion complex hydrogel-based scaffolds incorporating multi-walled carbon nanotubes using PME for bone regeneration. The hypothesis of the work was that the addition of multi-walled carbon nanotubes would enhance bone repair efficiency. It was observed that the fabricated scaffolds not only were biocompatible with rat bone marrow-derived mesenchymal stem cells, but also had a high degree of osteogenic differentiation, mineralized matrix formation, and osteogenesis upregulation.

2.2 Fused deposition modeling (FDM)

Similar to PME, FDM is a material extrusion AM process, which has been extensively utilized in tissue engineering applications. As illustrated in **Figure 5**, in the FDM process, a polymer/composite material, typically in the form of a filament, is fed into a heat block (maintained at a temperature above the melting temperature of the polymer material) with the aid of a stepper motor; this leads to formation of a molten polymer flow. A non-Newtonian fluid, the molten polymer is, subsequently, passed through a converging microcapillary nozzle (made up of, e.g., hardened steel or brass) in order to increase the linear momentum of the molten polymer flow

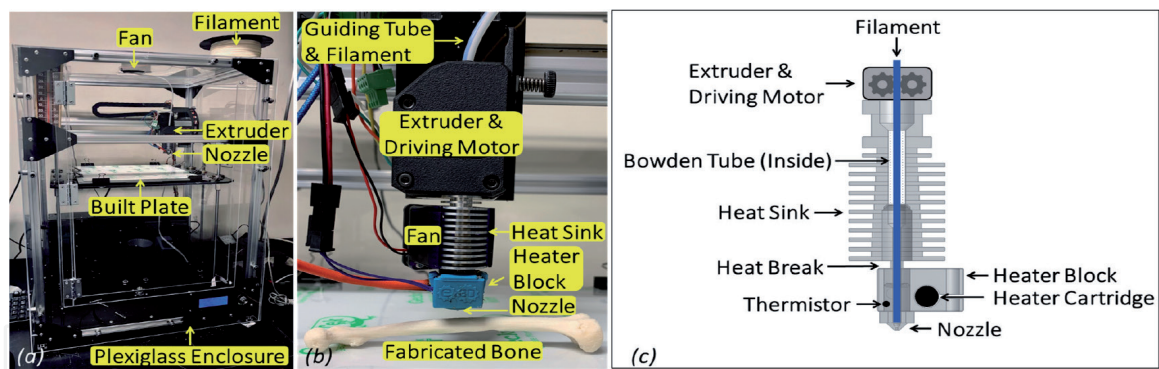


Figure 5. An FDM 3D-printing system, equipped with a Plexiglas enclosure and a fan installed to create a thermally uniform environment for steady-state material deposition. (a, b) Real pictures, and (c) a schematic diagram of the FDM deposition head assembly (Source: [1, 2, 22]).

prior to deposition on a heated or unheated free surface. Finally, the built plate (also known as platen) is automatically translated downward (controlled as a function of layer height), and the next layer is deposited on top of the previous layer. In fact, the layer height controls the amount of overlap between two subsequent deposited vertical layers. Please note that layer-to-layer bonding is influenced by not only the extrusion temperature, but also the layer height.

Chaffins et al. [1] investigated the mechanical properties of FDM-fabricated medical-grade bone scaffolds composed of a biocompatible composite material (with low moisture absorption) containing polyamide, polyolefin, and cellulose fibers. The composite material has an elongation at break, elasticity modulus (stiffness), and ultimate strength of 4%, 850 MPa, and 23 MPa, respectively. The FDM fabrication of the bone scaffolds was on the basis of a set of optimal process parameters, detailed in **Table 3**. An equilibration time of 3 hours was taken with the aim to ensure thermal equilibrium (regulated by the chamber fan) and as a result, steady-state material deposition in the FDM process. Please note that the fan speed affects the rate of material solidification after deposition. With the aid of a slicer software program, that is, Cura (Ultimaker, Utrecht, the Netherlands), the 3D CAD models of the bone scaffolds were converted into a G-code, and consequently a tool-path was created prior to fabrication.

The following research works exemplify the use of FDM in clinical practice. In a research work by Lai et al. [23], porous bone scaffolds with biomimetic structure were fabricated, based on a novel composite material composed of magnesium, PLGA, and β -tricalcium phosphate for the treatment of bone defects. A steroid-associated osteonecrosis rabbit model was established to assess the biosafety as well as the osteogenic and angiogenic properties of the fabricated scaffolds. It turned out that the scaffolds led to an increase in blood perfusion in addition to vessel ingrowth after surgery (approximately in 4–8 weeks), observed respectively with the aid of dynamic contrast-enhanced magnetic resonance imaging and micro-computed tomography (μ -CT)-based angiography. Furthermore, the fabricated scaffolds led to significant bone formation with enhanced functional properties.

Deng et al. [24] demonstrated additive fabrication of bi-lineage constructive scaffolds (composed of manganese-doped β -tricalcium phosphate) for bone regeneration. The physicochemical properties and bi-lineage bioactivity of the fabricated scaffolds as well as the mechanism of stimulating osteochondral regeneration were characterized. It was observed that the addition of manganese to β -tricalcium phosphate not only reduced the lattice parameters and

Parameter	Type	Level [unit]
Scaffold porosity (CAD-based)	Design	60 [%]
Number of shells	Design	1
Scaffold dimensions	Design	15 × 15 × 15 [mm]
Layer height (thickness)	Design	200 [μm]
Layer (line) width	Design	200 [μm]
Infill density	Design	100 [%]
Nozzle size	Machine	400 [μm]
Bed temperature	Machine	95 [°C]
Fan speed	Machine	83 [%] [10 Volts]
Print speed	Machine	15 [mm/s]
Deposition head temperature	Machine	235 [°C]
Flow (feed) rate	Machine	100 [%]
Steady state chamber temperature	Machine	37 [°C]
Build plate adhesion type	Machine	Brim

Table 3.

The optimal FDM process parameters used by Chaffins et al. for the additive fabrication of bone scaffolds composed of a biocompatible composite material. Please note that the bone scaffold fabrication process was based on the FT5-R₂ 3D-printing system (Folger Tech, Milford, NH, USA) (Source: [1]).

crystallization temperature, but also enhanced the density and the compressive strength of the fabricated scaffolds. The results of an animal study, in addition, showed that the ionic products from manganese-doped β-tricalcium phosphate improved the proliferation and promoted the differentiation of chondrocytes and rabbit mesenchymal stem cells. Furthermore, the results showed that the fabricated scaffolds significantly improved the regeneration of subchondral bone tissues, transplanted *in vivo*.

Hassanajili et al. [25] demonstrated characterization of polylactic-acid/polycaprolactone/hydroxyapatite composite scaffolds, fabricated using a combined fabrication process where material extrusion was utilized for the fabrication of a negative mold (composed of poly(vinyl alcohol), soluble in water) for casting integrated with freeze drying/particle leaching method. Liquid replacement technique was utilized to measure scaffold porosity. Cell adhesion, scaffold cytotoxicity, cell viability, and mineral deposition (indicative of osteoinductive capacity) together with modulus of elasticity, porosity, and pore size were measured to characterize the functional properties of the fabricated bone scaffolds.

Oladapo et al. [26] investigated the functional characteristics of biomimetic bone scaffolds, composed of poly lactic acid (PLA) matrix reinforced with carbohydrate particles and fabricated using the FDM process. In fact, the presence of carbohydrate particles allows for ion or ionic group substitutions and enhances the kinetics of absorption and ultimately, the mechanical properties of fabricated scaffolds. The bioactivity, surface roughness, apparent porosity, as well as mechanical properties of the fabricated scaffolds were analyzed. It was observed that there was a significant, proportional relationship between the carbohydrate content and surface roughness. In addition, the presence of carbohydrate particles led to a decline in scaffold stiffness and compressive strength (when compared with pure PLA).

2.3 Polymer jet printing (PJP)

Demonstrated in **Figure 6**, the PJP process operates on the basis of simultaneous deposition (jetting) of build as well as support materials (composed of liquid photopolymers) on a free surface [7]. Both build and support materials are radiation-curable. Having a resolution of, for example, 600 and 1200 dots per inch (DIP), inkjet heads are utilized for the deposition of liquid photopolymers onto a build platform. Subsequently, the deposited photopolymers are immediately cured *in situ* using a UV light source; this mechanism allows for fabrication of layers on top of each other. The photopolymer materials undergo a chemical transformation and become solid upon irradiation of the UV light [11].

Weese et al. [7] investigated the effects of four influential PJP process parameters, detailed in **Table 4**, on the mechanical properties of fabricated femur bone structures. The PJP process parameters include: (i) *print direction*, controlling the sequence of material deposition and layer formation; (ii) *resolution factor*, indicative of the resolution of material deposition; (iii) *UV light intensity*, controlling the intensity of the UV light source; and (iv) *deposition head temperature*.

The additive fabrication of the femur bone structures was based on a PJP 3D-printing system (Objet30 Pro, Stratasys Ltd., Eden Prairie, MN, USA), having an accuracy of 100 μm . The 3D-printing system, in addition, allows for deposition of materials with a layer thickness of as small as 28 μm . A slicer software program, that is, Objet Studio (Stratasys Ltd., Eden Prairie, MN, USA), was similarly used to convert 3D CAD models into a G-code and create a tool-path. The build photopolymer material used for the fabrication of the femur bone structures had a polymerized density, water absorption, and glass transition temperature (T_g) of 1.17–1.18 [g/cm^3], 1–1.5%, and 53°C, respectively. Furthermore, the build material had a

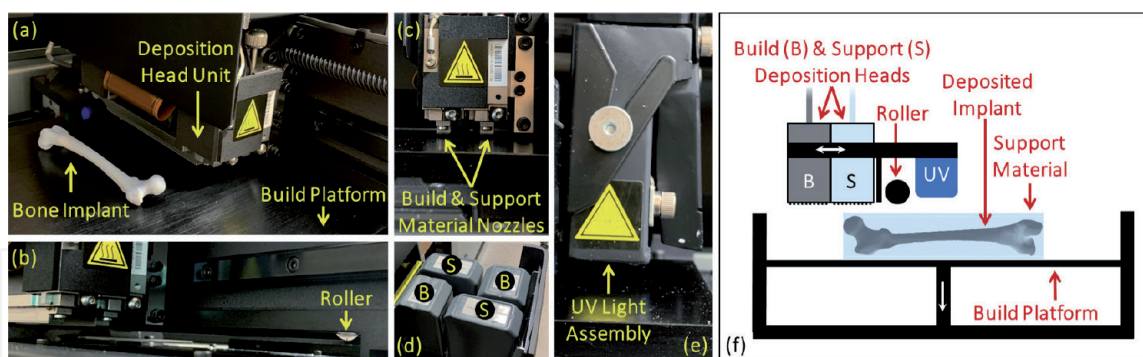


Figure 6. (a–e) Real pictures of the main components of the PJP process including: (a) the deposition head assembly; (b) the roller; (c) the material deposition nozzles; (d) the build and support material cartridges shown by the letters B and S, respectively; and (e) the UV light assembly. (f) A schematic diagram of the PJP process. Please note that the deposition head assembly includes build as well as support material nozzles (Source: [7]).

Parameter	Type	Level [unit]
Print direction	Machine	[Unidirectional, bidirectional]
Resolution factor	Machine	[0.25, 2.00]
UV light intensity factor	Machine	[0.34, 1.35]
Deposition head temperature factor	Machine	[0.65, 1.95]

Table 4. The PJP process parameters used by Weese et al. for the additive fabrication of femur bone structures (Source: [7]).

stiffness as well as a tensile strength of 2–3 GPa and 50–65 MPa, respectively. Unlike the build material, the support material was soluble in a solution of 2% sodium hydroxide (NaOH) and 1% sodium metasilicate (Na₂SiO₃).

The following research work exemplifies the use of PJP in clinical practice. In a research work by Libonati et al. [27], synthetic composite structures (composed of acrylic-based photopolymers and having a pattern inspired by the microstructure of cortical bone) were designed and characterized. The composite structures were fabricated using the PJP process, and their functional performance in terms of fracture behavior was characterized by mechanical testing. It was observed that the cortical bone-inspired design would potentially enhance toughness amplification and would be essential for balance with material strength. In addition, the PJ-fabricated composite structures showed similar cortical bone-related failure mechanisms, including crack deflection, crack branching, constrained microcracking, as well as fibril bridging.

2.4 Digital light processing (DLP)

DLP is a vat-photopolymerization AM process. It is, to some extent, similar to the PJP process, where radiation-curable resins become a solid upon exposure to UV light through a process called *photopolymerization*. **Figure 7** illustrates the main components of the DLP process. Once the first layer has been cured, the build platform is translated automatically upward, and the next layer is cured on top of the previous cured layer. The DLP process has been utilized for the high-resolution fabrication of 3D structures with complex internal geometries such as bone and dental implants. In a research work by Raines et al. [28], dental implants with complex internal structures were fabricated using the DLP process. The fabricated dental implants were composed of a biocompatible resin. The DLP process consists of several design and process parameters, as listed in **Table 5**. 3D-Sprint (3D Systems, Rock Hill, SC, USA) was the slicer software program of choice. Finally, the DLP 3D-printing system used in their work was FabPro 1000 (3D Systems, Rock Hill, SC, USA).

2.5 A review of other AM processes used in clinical practice

2.5.1 Powder bed fusion

Pei et al. [29] demonstrated an integrated method for the biomechanical design as well as fabrication of bionic bone tissue implants using SLS additive

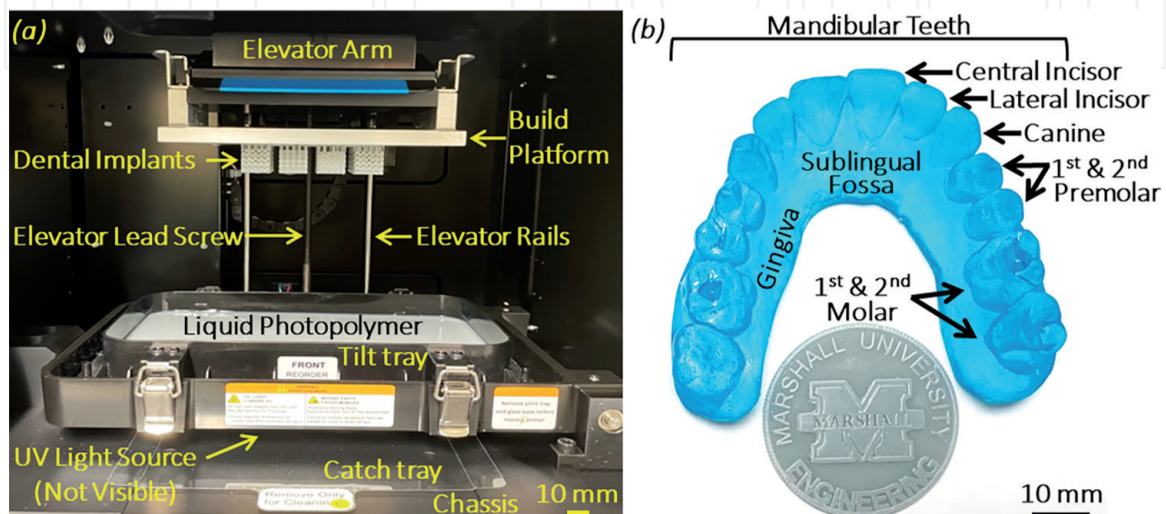


Figure 7. (a) The main components of the DLP additive manufacturing process. (b) An X-ray microCT-based, biocompatible dental jaw model, fabricated using the DLP-AM process (Source: [28]).

Parameter	Type	Level [unit]
Scaffold porosity	Design	60 [%]
Number of shells	Design	1
Scaffold dimensions	Design	15 × 15 × 15 [mm]
Layer thickness	Design	100 [μm]
Cure depth	Machine	115 [μm]
Print resolution	Machine	454 × 454 dpi
Layer resolution	Machine	100 [μm]

Table 5. The DLP process parameters used by Raines et al. for the fabrication of dental structures, composed of a biocompatible liquid photopolymer (Source: [28]).

manufacturing process with the aim to repair the femoral head. Composed of titanium, the fabricated implants were based on interconnected diamond-lattice pore units that would prevent stress shielding. FEA was utilized for design optimization and numerical characterization of the mechanical properties of the bone implants. On the basis of an animal study, it was observed that pore-unit parameters would significantly influence implant porosity, pore size distribution, and mechanical strength.

Zhang et al. [30] designed and fabricated porous scaffolds (composed of Ti6Al4V alloy and having diamond-lattice pore units with customized shape and tunable mechanical properties) using SLS process for bone tissue regeneration and ultimately femoral-head repair. The weak points within the structure of the scaffolds were analyzed using a FEA model. Struts diameters, pore size, as well as porosity were identified as critical implant design parameters. The biocompatibility and osteogenic potential of the fabricated scaffolds were assessed *in vivo* based on an animal study.

Similarly, Zhao et al. [31] investigated the mechanical properties of porous titanium alloy scaffolds fabricated using SLS process for bone tissue reconstruction. Various scaffolds (including Diamond, Gyroid, Orthogonal, Truss, and Cube) were designed based on parameterization modeling. The mechanical characteristics of the designs as well as the SLS-fabricated scaffolds were assessed numerically using FEA and experimentally using mechanical testing, respectively. It was observed that the fabricated scaffolds were dimensionally accurate characterized with an error of <3% (when compared with their reference CAD models).

2.5.2 Binder jetting

In a research work by Inzana et al. [32], composite bone scaffolds (composed of calcium phosphate and collagen) were fabricated using binder jet additive manufacturing process. Collagen was dissolved into a phosphoric acid-based binder solution to synthesize a collagen-incorporated calcium phosphate composite. The addition of collagen, to a great extent, improved the flexural strength of the fabricated scaffolds as well as cell viability. In addition, it was observed that the properties of the binder solution would play a significant role in the cytocompatibility, osteoconductivity, and mechanical strength of the fabricated bone scaffolds. Furthermore, to achieve reliable material deposition, the viscosity and surface tension of the collagen solution were reduced with the aid of physiologic heat treatment and Tween 80, respectively. To assess the healing potential, the fabricated

scaffolds were implanted into a critically-sized murine femoral defect for 9 weeks; it turned out that the implants not only were osteoconductive, but also led to new bone growth.

Zhou et al. [33] investigated the characteristics of synthesized composite materials composed of calcium phosphate powders (based on hydroxyapatite and β -tricalcium phosphate) as well as calcium sulfate powders for the fabrication of bone scaffolds using binder jet printing process (with a water-based binder). The printability of the composite materials was assessed in terms of powder bed packing, binder deposition regimes, particle size, calcium phosphate:calcium sulfate ratio, powder-binder wettability, and the strength of the fabricated scaffolds. It was observed that the compressive strength of the scaffolds increased as the ratio of calcium phosphate:calcium sulfate increased. In addition, the use of fine powders (i.e., $\leq 20 \mu\text{m}$ in diameter) led to slow binder penetration rate, large penetration depth, low wetting ratio, and insignificant green-state strength. Besides, the beta tricalcium phosphate-based powders had lower wetting ratio as well as green-state strength than the hydroxyapatite-based powders.

Bergmann et al. [34] demonstrated additive fabrication of customized bone substitute implants composed of bioresorbable β -tricalcium phosphate as well as bioresorbable and adjustable bioactive glass fabricated using binder jet printing process for swift maxillofacial or craniofacial defect repair. The fabricated scaffolds had a bending strength of approximately 15 MPa. In addition, the results of an X-ray powder diffraction (XRD) analysis revealed the presence of both calcium sodium phosphate and calcium silicate (that are biocompatible and biodegradable).

Similarly, Cox et al. [35] presented characterization of porous bone scaffolds, fabricated using binder jet printing process and composed of hydroxyapatite as well as poly(vinyl)alcohol (PVOH) composite powders (bound with the aid of a water-based binding agent). It was observed that scaffold mechanical stability, microstructure, and porosity would be significantly affected by the flowability of hydroxyapatite:PVOH precursor materials. The fabricated scaffolds were anisotropic, and failure at the boundaries of interlayer bonds was identified as the primary failure mechanism influencing the scaffolds' functional performance. Furthermore, it turned out that *in vivo* osteoconduction and osteointegration would be significantly enhanced by factors, such as scaffold porosity and interconnectivity in addition to powder bed packing and surface roughness.

3. Conclusions

In this chapter, advanced AM processes were analyzed with a focus on PME, FDM, PJP, as well as DLP. In addition, each AM process was characterized in terms of system components, underlying physical phenomena, and influential parameters. The AM processes are inherently complex, despite their benefits and engendered potential applications. The process complexity, to a great extent, stems from complex physical phenomena (such as non-Newtonian material deposition and phase change) as well as nonlinear material-process interactions. Furthermore, the 3D fabrication of bone tissue scaffolds and implants consists of a broad spectrum of design and process parameters, for example, scaffold porosity, material viscosity, and UV light intensity. Hence, investigation of the effects of the process parameters integrated with physics-based process characterization using computational methods, such as CFD and FEA, would be an inevitable need toward obtaining optimal material transport and deposition regimes for the fabrication of bone tissues with tunable medical properties.

Acknowledgements

This work was made possible by the NASA Established Program to Stimulate Competitive Research (EPSCoR), Grant # 80NSSC19M0054. Dr. Salary would like to sincerely thank the NASA West Virginia Space Grant Consortium (Morgantown, WV, USA). In addition, Dr. Salary would like to sincerely acknowledge the Marshall University Research Corporation (MURC) for supporting this work via the John Marshall Scholars Faculty Award. Furthermore, Dr. Salary would like to sincerely thank the West Virginia State's Higher Education Policy Commission and the Community and Technical College System for the Open Education Resources (OER) Grant.

Dr. Salary also would like to thank the College of Engineering & Computer Sciences (CECS) at Marshall University, the Cabell Huntington Hospital and Medical Center (Huntington, WV, USA), as well as FibreTuff Biotechnology Company (Toledo, OH, USA).

Nomenclatures

AJP	aerosol jet printing
AM	additive manufacturing
CAD	computer-aided design
CFD	computational fluid dynamics
DHT	deposition head temperature
DLP	digital light processing
FDM	fused deposition modeling
FEA	finite element analysis
PCL	polycaprolactone
PJP	polymer jet printing
PME	pneumatic micro-extrusion
SLS	selective laser sintering

IntechOpen


Author details

Roozbeh (Ross) Salary

Departments of Mechanical and Biomedical Engineering, College of Engineering and Computer Sciences, Marshall University, Huntington, WV, USA

*Address all correspondence to: salary@marshall.edu

IntechOpen

© 2022 The Author(s). Licensee IntechOpen. This chapter is distributed under the terms of the Creative Commons Attribution License (<http://creativecommons.org/licenses/by/3.0>), which permits unrestricted use, distribution, and reproduction in any medium, provided the original work is properly cited. 

References

- [1] Chaffins A, Yu M, Claudio PP, Day JB, Salary RR. Investigation of the functional properties of additively-fabricated triply periodic minimal surface-based bone scaffolds for the treatment of osseous fractures. In: Proc. Paper No. 2004, ASME 2021 International Manufacturing Science and Engineering Conference (MSEC 2021), Virtual Conference (Due to the COVID-19 Pandemic); 21-25 June 2021; University of Cincinnati, Cincinnati, OH, USA. American Society of Mechanical Engineers
- [2] Zhao D, Hart C, Weese NA, Rankin CM, Kuzma J, Day JB, Salary RR. Experimental and computational analysis of the mechanical properties of biocompatible bone scaffolds, fabricated using fused deposition modeling additive manufacturing process. In: Proc. Paper No. 8511, ASME 2020 International Manufacturing Science and Engineering Conference (MSEC 2020); 22-26 June 2020; Cincinnati, OH, USA. American Society of Mechanical Engineers. DOI:10.1115/MSEC2020-8511
- [3] Klemstine C, Abdelgaber Y, Lawrence L, Day JB, Claudio PP, Salary RR. Characterization of the compressive properties of triply periodic minimal surface (TPMS) polycaprolactone scaffolds for bone tissue engineering. In: Proc. Paper No. IMECE2021-72125, ASME International Mechanical Engineering Congress & Exposition (IMECE 2021), Virtual Conference; 1-5 November 2021. American Society of Mechanical Engineers
- [4] Yu M, Yeow YJ, Lawrence L, Claudio PP, Day JB, Salary R. Characterization of the functional properties of PCL bone scaffolds fabricated using pneumatic microextrusion. *Journal of Micro and Nano-Manufacturing*. 2021;9(3):030905 (13 Pages). DOI: 10.1115/1.4051631
- [5] Zhao D, Yu M, Lawrence L, Claudio PP, Day JB, Salary RR. Investigation of the influence of consequential design parameters on the mechanical performance of biodegradable bone scaffolds, fabricated using pneumatic micro-extrusion additive manufacturing process. In: Proc. Paper No. 8512, ASME 2020 International Manufacturing Science and Engineering Conference (MSEC 2020); 22-26 June 2020; Cincinnati, OH, USA. American Society of Mechanical Engineers. DOI:10.1115/MSEC2020-8512
- [6] Lawrence L, Day JB, Claudio PP, Salary RR. Investigation of the regenerative potential of human bone marrow stem cell-seeded polycaprolactone bone scaffolds, fabricated using pneumatic microextrusion process. In: Proc. Paper No. 1997, ASME 2021 International Manufacturing Science and Engineering Conference (MSEC 2021); 21-25 June 2021; University of Cincinnati, Cincinnati, OH, USA. American Society of Mechanical Engineers. DOI:10.1115/MSEC2021-63411
- [7] Weese NA, Rankin CM, Zhao D, Hart C, Quinlan P, Day JB, Salary RR. Experimental optimization of polymer jetting additive manufacturing process using Taguchi design. In: Proc. Paper No. IMECE2020-24271, V02AT02A046, 7 Pages, ASME 2020 International Mechanical Engineering Congress and Exposition (IMECE 2020); 16-19 November 2020. American Society of Mechanical Engineers. DOI:10.1115/IMECE2020-24271
- [8] Yeow YJ, Yu M, Day JB, Salary RR. A computational fluid dynamics (CFD) study of material flow in pneumatic microextrusion (PME) additive manufacturing process. In: Proc. Paper No. 24325, ASME 2020 International Mechanical Engineering Congress and Exposition (IMECE2020); 16-19

November 2020; Portland, OR, USA. American Society of Mechanical Engineers. DOI:10.1115/IMECE2020-24325

[9] Yu M, Lawrence L, Claudio PP, Day JB, Salary RR. Pneumatic microextrusion-based additive biofabrication of polycaprolactone bone scaffolds—part II: Investigation of the influence of polymer flow parameters. In: Proc. Paper No. 2002, ASME 2021 International Manufacturing Science and Engineering Conference (MSEC 2021), Virtual Conference (Due to the COVID-19 Pandemic); 21-25 June 2021; University of Cincinnati, Cincinnati, OH, USA. American Society of Mechanical Engineers

[10] Yu M, Yeow YJ, Lawrence L, Claudio PP, Day JB, Salary RR. Investigation of the effects of design and process parameters on the mechanical properties of biodegradable bone scaffolds, fabricated using pneumatic microextrusion process. In: Proc. Paper No. 24252, ASME 2020 International Mechanical Engineering Congress and Exposition (IMECE2020). 16-19 November 2020; Portland, OR, USA. American Society of Mechanical Engineers. DOI:10.1115/IMECE2020-24252

[11] Gibson I, Rosen DW, Stucker B. Additive Manufacturing Technologies—3D Printing, Rapid Prototyping, and Direct Digital Manufacturing. New York, NY, USA: Springer; 2014. DOI: 10.1007/978-1-4939-2113-3

[12] Spoerk M, Gonzalez-Gutierrez J, Sapkota J, Schuschnigg S, Holzer C. Effect of the printing bed temperature on the adhesion of parts produced by fused filament fabrication. *Plastics, Rubber and Composites*. 2018;**47**(1):17-24. DOI: 10.1080/14658011.2017.1399531

[13] Jenkins M, Stamboulis A. Durability and Reliability of Medical Polymers.

Philadelphia, PA, USA: Woodhead Publishing; 2012

[14] Salary R, Lombardi JP, Tootooni MS, Donovan R, Rao PK, Borgesen P, et al. Computational fluid dynamics modeling and online monitoring of aerosol jet printing process. *Journal of Manufacturing Science and Engineering*. 2017;**139**(2):021015. DOI: 10.1115/1.4034591

[15] Salary R, Lombardi JP, Tootooni MS, Donovan R, Rao PK, Poliks MD. *In situ* sensor-based monitoring and computational fluid dynamics (CFD) modeling of aerosol jet printing (AJP) process. In: Proc. Paper No. 8535, ASME 2016 11th International Manufacturing Science and Engineering Conference (MSEC 2016); 27 June–1 July 2016; Virginia Tech, Blacksburg, VA, USA. American Society of Mechanical Engineers. p. V002T004A049. DOI:10.1115/MSEC2016-8535

[16] Salary R, Lombardi JP, Weerawarne DL, Rao PK, Poliks MD. A computational fluid dynamics (CFD) study of material transport and deposition in aerosol jet printing (AJP) process. In: Proc. Paper No. 87647, ASME 2018 International Mechanical Engineering Congress & Exposition (IMECE 2018); 9-15 November 2018; Pittsburgh, PA, USA. American Society of Mechanical Engineers. DOI:10.1115/IMECE2018-87647

[17] Salary R, Lombardi JP, Weerawarne DL, Rao P, Poliks MD. A computational fluid dynamics investigation of pneumatic atomization, aerosol transport, and deposition in aerosol jet printing process. *Journal of Micro and Nano-Manufacturing*. 2021;**9**(1):010903. DOI: 10.1115/1.4049958

[18] Du X, Wei D, Huang L, Zhu M, Zhang Y, Zhu Y. 3D printing of mesoporous bioactive glass/silk fibroin composite scaffolds for bone tissue engineering. *Materials Science and*

Engineering: C. 2019;**103**:109731.
DOI: 10.1016/j.msec.2019.05.016

[19] Du X, Yu B, Pei P, Ding H, Yu B, Zhu Y. 3D printing of pearl/CaSO₄ composite scaffolds for bone regeneration. *Journal of Materials Chemistry B*. 2018;**6**(3):499-509.
DOI: 10.1039/C7TB02667F

[20] Park JY, Shim J-H, Choi S-A, Jang J, Kim M, Lee SH, et al. 3D printing technology to control BMP-2 and VEGF delivery spatially and temporally to promote large-volume bone regeneration. *Journal of Materials Chemistry B*. 2015;**3**(27):5415-5425.
DOI: 10.1039/C5TB00637F

[21] Cui H, Yu Y, Li X, Sun Z, Ruan J, Wu Z, et al. Direct 3D printing of a tough hydrogel incorporated with carbon nanotubes for bone regeneration. *Journal of Materials Chemistry B*. 2019;**7**(45):7207-7217.
DOI: 10.1039/C9TB01494B

[22] E3D-v6 Assembly. Open Source Creative Commons (CC BY-NC-SA 3.0) License, UK. Available from: <https://e3d-online.dozuki.com/>

[23] Lai Y, Li Y, Cao H, Long J, Wang X, Li L, et al. Osteogenic magnesium incorporated into PLGA/TCP porous scaffold by 3D printing for repairing challenging bone defect. *Biomaterials*. 2019;**197**:207-219. DOI: 10.1016/j.biomaterials.2019.01.013

[24] Deng C, Yao Q, Feng C, Li J, Wang L, Cheng G, et al. Retracted: 3D printing of bilineage constructive biomaterials for bone and cartilage regeneration. *Advanced Functional Materials*. 2017;**27**(36):1703117.
DOI: 10.1002/adfm.201703117

[25] Hassanajili S, Karami-Pour A, Oryan A, Talei-Khozani T. Preparation and characterization of PLA/PCL/HA composite scaffolds using indirect 3D printing for bone tissue engineering.

Materials Science and Engineering: C. 2019;**104**:109960. DOI: 10.1016/j.msec.2019.109960

[26] Oladapo BI, Zahedi S, Adeoye A. 3D printing of bone scaffolds with hybrid biomaterials. *Composites Part B: Engineering*. 2019;**158**:428-436.
DOI: 10.1016/j.compositesb.2018.09.065

[27] Libonati F, Gu GX, Qin Z, Vergani L, Buehler MJ. Bone-inspired materials by design: Toughness amplification observed using 3D printing and testing. *Advanced Engineering Materials*. 2016;**18**(8):1354-1363. DOI: 10.1002/adem.201600143

[28] Raines R, Day JB, Salary RR. Experimental characterization of the mechanical properties of medical-grade dental implants, fabricated using vat-photopolymerization additive manufacturing process. In: Proc. Paper No. 85436, ASME 2022 International Manufacturing Science and Engineering Conference (MSEC 2022); 27 June–1 July 2022; Purdue University, West Lafayette, IN, USA. American Society of Mechanical Engineers

[29] Pei X, Zhang B, Fan Y, Zhu X, Sun Y, Wang Q, et al. Bionic mechanical design of titanium bone tissue implants and 3D printing manufacture. *Materials Letters*. 2017;**208**:133-137. DOI: 10.1016/j.matlet.2017.04.128

[30] Zhang B, Pei X, Zhou C, Fan Y, Jiang Q, Ronca A, et al. The biomimetic design and 3D printing of customized mechanical properties porous Ti6Al4V scaffold for load-bearing bone reconstruction. *Materials and Design*. 2018;**152**:30-39. DOI: 10.1016/j.matdes.2018.04.065

[31] Zhao L, Pei X, Jiang L, Hu C, Sun J, Xing F, et al. Bionic design and 3D printing of porous titanium alloy scaffolds for bone tissue repair. *Composites Part B: Engineering*. 2019;**162**:154-161. DOI: 10.1016/j.compositesb.2018.10.094

[32] Inzana JA, Olvera D, Fuller SM, Kelly JP, Graeve OA, Schwarz EM, et al. 3D printing of composite calcium phosphate and collagen scaffolds for bone regeneration. *Biomaterials*. 2014;**35**(13):4026-4034. DOI: 10.1016/j.biomaterials.2014.01.064

[33] Zhou Z, Buchanan F, Mitchell C, Dunne N. Printability of calcium phosphate: Calcium sulfate powders for the application of tissue engineered bone scaffolds using the 3D printing technique. *Materials Science and Engineering: C*. 2014;**38**:1-10. DOI: 10.1016/j.msec.2014.01.027

[34] Bergmann C, Lindner M, Zhang W, Koczur K, Kirsten A, Telle R, et al. 3D printing of bone substitute implants using calcium phosphate and bioactive glasses. *Journal of the European Ceramic Society*. 2010;**30**(12):2563-2567. DOI: 10.1016/j.jeurceramsoc.2010.04.037

[35] Cox SC, Thornby JA, Gibbons GJ, Williams MA, Mallick KK. 3D printing of porous hydroxyapatite scaffolds intended for use in bone tissue engineering applications. *Materials Science and Engineering: C*. 2015;**47**:237-247. DOI: 10.1016/j.msec.2014.11.024